

Expression of antisense uPAR and antisense uPA from a bicistronic adenoviral construct inhibits glioma cell invasion, tumor growth, and angiogenesis

Christopher S Gondi¹, Sajani S Lakka¹, Niranjan Yanamandra¹, Khawar Siddique², Dzung H Dinh², William C Olivero², Meena Gujrati³ and Jasti S Rao^{*1,2}

¹Division of Cancer Biology, Department of Biomedical and Therapeutic Sciences, University of Illinois, Peoria, IL, USA;

²Department of Neurosurgery, University of Illinois, Peoria, IL, USA; ³Department of Pathology, University of Illinois Peoria, IL, USA

Urokinase-type plasminogen activator (uPA) and its receptor (uPAR) play an important role in the invasiveness of gliomas and other infiltrative tumors. In glioma cell lines and tumors, high grade correlates with increased expression of uPAR and uPA. We report here the downregulation of uPAR and uPA by delivery of antisense sequences of uPAR and uPA in a single adenoviral vector, Ad-uPAR-uPA (Ad, adenovirus). The bicistronic construct (Ad-uPAR-uPA) infected glioblastoma cell line had significantly reduced levels of uPAR, uPA enzymatic activity and immunoreactivity for these proteins when compared to controls. The Ad-uPAR-uPA infected cells showed a markedly lower level of invasion in the Matrigel invasion assays, and their spheroids failed to invade the fetal rat brain aggregates in the coculture system. Intracranial injection of SNB19 cells with the Ad-uPAR-uPA antisense bicistronic construct showed inhibited invasiveness and tumorigenicity. Subcutaneous injections of bicistronic antisense constructs into established tumors (U87 MG) caused regression of those tumors. Our results support the therapeutic potential of targeting the individual components of the uPAR-uPA system by using a single adenovirus construct for the treatment of glioma and other invasive cancers.

Oncogene (2003) 22, 5967–5975. doi:10.1038/sj.onc.1206535

Keywords: adenovirus; antisense; glioma; invasion; uPA and uPAR

Introduction

Urokinase and its high-affinity receptor, a glycosyl phosphatidylinositol-anchored membrane protein

(CD87), are believed to be critical elements in tumor biology since they control cell motility, tissue remodeling, and the bioavailability of angiogenic factors. Formation of the uPA–uPAR complex at the cell surface is required for efficient activation of plasmin, a protease that can degrade the components of the extracellular matrix (ECM) (Ellis and Dano, 1993). uPA is a 52-kDa serine protease secreted as an inactive single-chain proenzyme (pro-uPA) that is efficiently converted to an active two-chain uPA by plasmin (Nielsen *et al.*, 1982). Two-chain uPA in turn is a potent activator of plasminogen, leading to a powerful feedback loop that results in productive plasmin formation (Bugge *et al.*, 1996). However, both pro-uPA and plasminogen are catalytically inactive proenzymes and the mechanism by which uPA-mediated plasminogen activation is initiated is not fully understood. Although many studies have documented that uPAR has a central role in uPA-mediated cell surface plasminogen activation, recent studies with uPAR-deficient mice have demonstrated the existence of additional pathways of uPA-mediated plasminogen activation that are independent of uPAR. These additional pathways participate in physiological cell migration and fibrin dissolution (Bugge *et al.*, 1996; Carmeliet *et al.*, 1998). For effective invasion, the precise distribution of uPAR apparently concentrates uPA at the leading edge of migrating cells, generating a fully activated proteolytic cascade in front of the invading tumor. The relevance of targeting uPA and uPAR for cancer therapy is supported by epidemiologic studies in which high-level expression of uPA and uPAR correlated with poor prognosis in several malignancies, including breast, stomach, brain, and lung (Sappino *et al.*, 1987; Schmitt *et al.*, 1992; Kobayashi *et al.*, 1993; Yamamoto *et al.*, 1994a, b; Foekens *et al.*, 1995; Park *et al.*, 1997). Recently, we reported that downregulation of the uPAR level by using an antisense strategy involving an adenovirus construct inhibited glioma invasion *in vitro* and glioma tumor formation *in vivo* (Mohan *et al.*, 1999). Other reports indicated that downregulating uPAR expression with an antisense strategy induced a protracted period of dormancy, causing cells to be arrested at G₀/G₁ *in vivo*, but did

*Correspondence: JS Rao, Division of Cancer Biology, Department of Biomedical and Therapeutic Sciences, The University of Illinois College of Medicine at Peoria, Peoria, IL 61656, USA; E-mail: jsrao@uic.edu

Supported by National Cancer Institute Grant CA 75557 (to JSR)
Received 31 December 2002; revised 19 February 2003; accepted 26 February 2003

not affect their growth *in vitro* (Yu *et al.*, 1997; Adachi *et al.*, 2002). The expression of uPAR by human glioblastoma cells probably contributes to their invasive capacity (Mohanam *et al.*, 1993). Hence, a direct reduction in both uPAR and uPA levels would significantly retard the invasiveness of a glioma. In the present study, we constructed a bicistronic, replication-deficient adenovirus vector containing antisense uPAR and antisense uPA with the intent of downregulating both uPAR and uPA levels in human gliomas. We examined the biological activity of this Ad-uPAR-uPA construct in human glioma cell lines, both *in vitro* and *in vivo*.

Results

Ad-uPAR-uPA infection decreased uPAR protein levels and uPA activity in the glioblastoma cell line SNB19

Western blot analysis was performed to examine the effect of Ad-uPAR-uPA infection on uPAR protein levels in SNB19 cells. Figure 1a shows that the uPAR protein band (MR 60 000) decreased in a dose-depen-

dent fashion as the multiplicities of infection (MOI) increased. Quantification of uPAR protein bands on Western blots by densitometry showed a significant ($P < 0.001$) decrease in the cells infected with Ad-uPAR-uPA at 25 MOI. For cells infected with Ad-uPAR-uPA at an MOI of 50, this decrease reached more than 90% when compared to Ad-CMV-infected control cells (CMV, cytomegalovirus). Figure 1a also showed that the Ad-uPAR antisense construct also decreased the levels of uPAR, as is consistent with our earlier report (Mohan *et al.*, 1999), but this effect was much less when compared with the bicistronic construct (Ad-uPAR-uPA). Figure 1b shows that the decrease in the uPAR protein level was related to time; that is the SNB19 cells infected with Ad-uPAR-uPA at 100 MOI showed an 80% decrease in uPAR level by day 4. The β -actin levels did not change under any of the above conditions, indicating that a similar amount of protein had been loaded in each lane.

Fibrin zymography

Fibrin zymography was performed to examine the effect of Ad-uPAR-uPA infection on uPA enzymatic activity

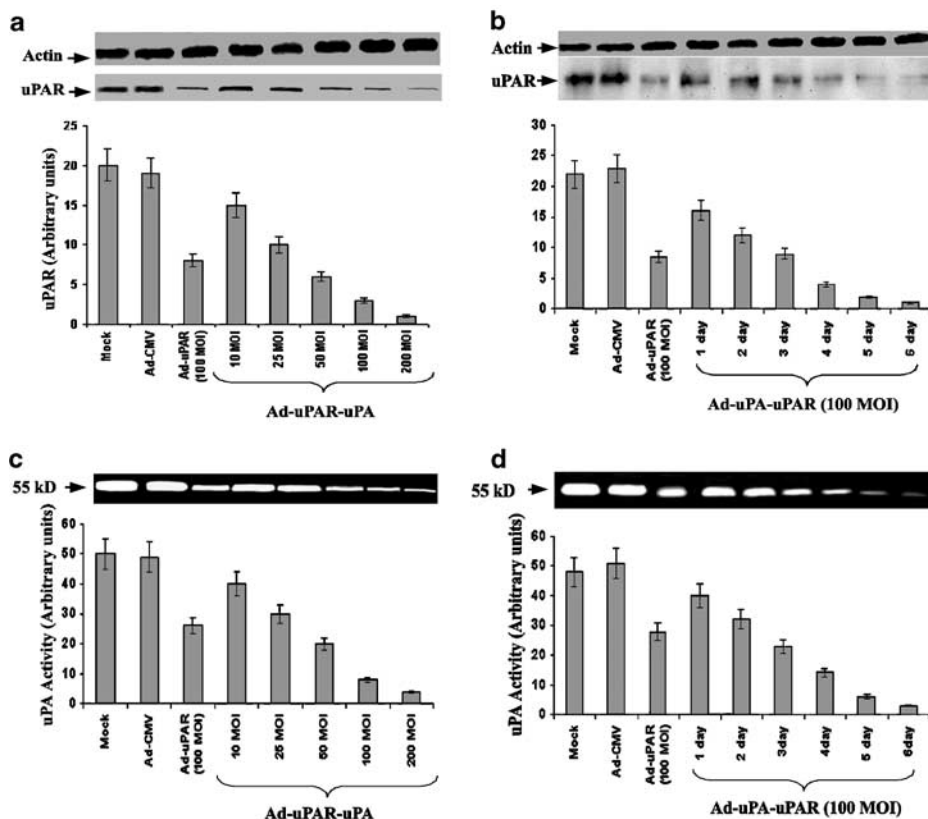


Figure 1 Western blot analysis of uPAR and fibrin zymography for uPA. SNB19 cells infected with Ad-CMV, Ad-uPAR and Ad-uPAR-uPA for 4 days at the indicated MOI and uPAR levels were determined by Western blotting (a). SNB19 cells infected with Ad-CMV, Ad-uPAR, and Ad-uPAR-uPA at 100 MOI at the indicated time points and uPAR protein levels were determined by Western blotting (b). Cell-bound uPA activity of SNB19 cells infected with Ad-CMV, Ad-uPAR and Ad-uPAR-uPA for 6 days in serum-free medium at the indicated MOI as determined by fibrin zymography (c). Cell-bound uPA activity of SNB19 cells infected with Ad-CMV, Ad-uPAR and Ad-uPAR-uPA at 100 MOI at the indicated time points as determined by fibrin-zymography (d). Protein levels of uPAR and uPA activity on Western blots and fibrin zymography were quantified by densitometry and the data are presented as mean values from four separate experiments. (\pm s.d.; $P < 0.001$). In addition β actin antibodies were used to verify that similar amounts of protein had been loaded in each lane. Arbitrary units were calculated differently for uPAR and uPA

in SNB19 cells. Figure 1c shows that the uPA enzymatic activity (MR 55 000) decreased in a dose-dependent fashion as the MOI increased. Densitometric quantification of the uPA enzymatic activity on the fibrin zymograms showed a significant decrease in the cells infected with Ad-uPAR-uPA at an MOI of 50. This decrease reached more than 90% of the cells infected with Ad-uPAR-uPA at an MOI of 200 (with the percentage decrease determined relative to those in Ad-CMV-infected control cells). The decrease in uPA enzymatic activity also was related to time as SNB19 cells infected with 100 MOI of Ad-uPAR-uPA showed a 90% decrease in uPA activity by day 5 (Figure 1d).

Ad-uPAR-uPA infection decreased uPAR and uPA immunoreactivity and angiogenesis

Immunohistochemical analysis was performed to examine the effect of Ad-uPAR-uPA infection on uPA and

uPA protein intensity in SNB19 cells. Figure 2 shows the expression of uPAR and uPA protein levels in mock, Ad-CMV, Ad-uPAR and Ad-uPAR-uPA infected cells via the use of specific antibodies for uPAR and uPA. The intensity of this staining for uPAR and uPA was much less in Ad-uPAR and Ad-uPAR-uPA infected cells when compared to mock- or Ad-CMV infected control cells. The effect of the bicistronic antisense construct (Ad-uPAR-uPA) or single antisense adenoviral construct (Ad-uPAR) to regulate angiogenesis in tumors was tested by coculturing human endothelial cells with SNB19 cells. The endothelial cells formed capillary-like structures within 24–48 h in the presence of SNB19 cells. Increasing the MOI of the bicistronic vector progressively inhibited capillary-like structures in a dose-dependent manner (Figure 2b). The effect of the bicistronic construct to inhibit capillary-like structures was much higher when compared to Ad-uPAR-, Ad-CMV and mock-infected cocultures.

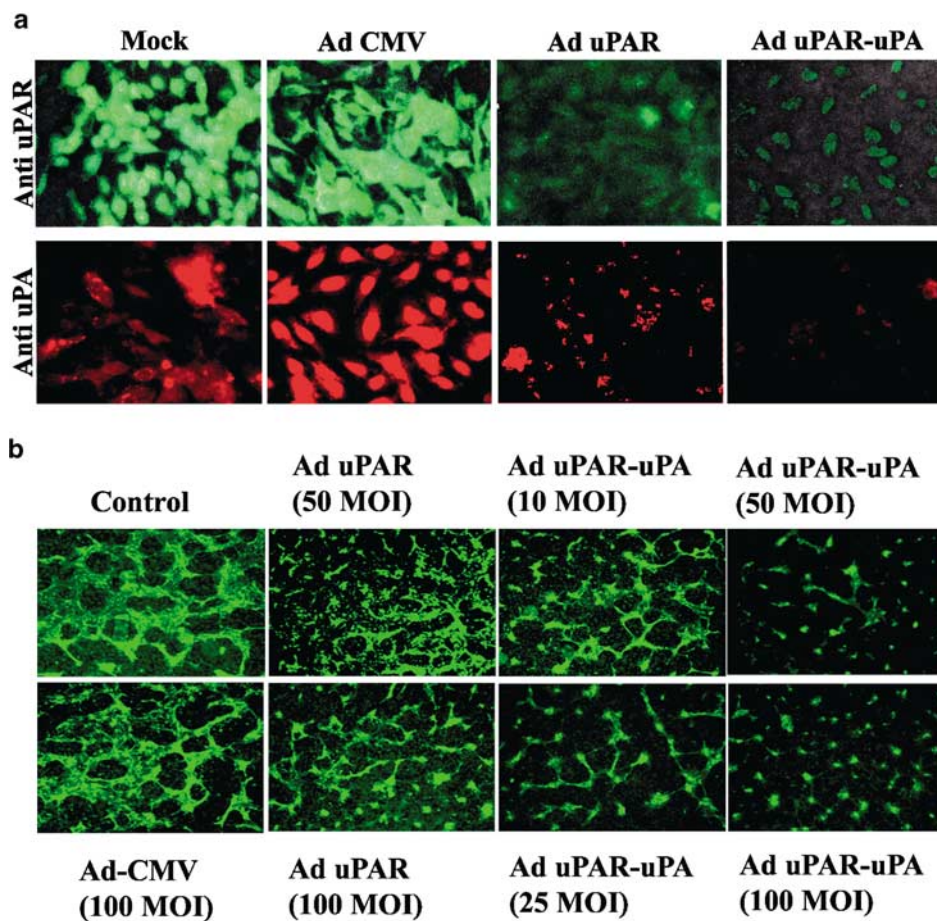


Figure 2 Ad-uPAR-uPA infection decreased uPAR and uPA protein levels as shown by immunohistochemical analysis (a). SNB19 cells (1×10^4) were seeded in eight-well chamber slides, incubated for 24 h, and infected with 100 MOI of Ad-CMV, Ad-uPAR or Ad-uPAR-uPA. After 72 h, cells were fixed, washed for 1 h with blocking buffer and stained for uPAR and uPA using specific antibodies for either uPAR or uPA. Ad-uPAR-uPA inhibited tumor-induced angiogenesis (b). SNB19 cells (2×10^4) were seeded in eight-well chamber slides and infected with indicated MOI of Ad-CMV, Ad-uPAR and Ad-uPAR-uPA. After 24 h incubation, the medium was removed and the cells were cocultured with 4×10^4 human endothelial cells. After 72 h, endothelial cells were stained for factor VIII antigen and examined under a confocal scanning laser microscope

Ad-uPAR-uPA infection decreased cellular migration from spheroids

Spheroids composed of the mock-infected control cells showed significant migration of cells from the spheroids, which was comparable to the migration from spheroids composed of cells infected with Ad-CMV. The migration of cells from Ad-uPAR-uPA-infected spheroids showed significantly less migration when compared to Ad-CMV and mock controls. The effect of Ad-uPAR-uPA construct showed neither attachment to the chamber slides nor migration of cells from the spheroids (Figure 3a) and the effect is dose dependent.

Ad-uPAR-uPA infection decreased invasiveness of SNB19 cells

The effect of downregulation of uPAR and uPA levels by Ad-uPAR-uPA infection on the invasiveness of SNB19 cells was studied using a Matrigel model that compared the invasion of infected cells through matrigel coated filters with that of mock and Ad-CMV controls. When cells were seeded at a density of 1×10^6 cells/ml in the upper chamber, the staining of Ad-uPAR- or Ad-uPAR-uPA-transfected cells that invaded through the

Matrigel was significantly less compared to mock-infected and Ad-CMV-infected cells (Figure 3b). Quantitative analysis of the number of cells invaded through the Matrigel in mock- and Ad-CMV-infected SNB19 cells was considered 100%. Therefore, only 25% and 10% of cells invaded through the Matrigel in Ad-uPAR- and Ad-uPAR-uPA-infected cells. The effect of Ad-uPAR-uPA infection on the invasiveness of SNB19 was also studied using a spheroid model. In these experiments, the invasion of Ad-uPAR-uPA-transfected cells into fetal rat brain aggregates was compared with that of cells infected with Ad-CMV. The invasion of glioma spheroids infected with Ad-CMV during cocultures with fetal rat brain aggregates (Figure 4a). Glioma spheroids infected with Ad-CMV progressively invaded by approximately 90–95% at 72 h. However, glioma spheroids infected with Ad-uPAR-uPA at 25, 50 and 100 MOI in cocultures with fetal rat brain aggregates invaded by only 15–5% at 72 h. These results show that the bicistronic construct containing both antisense molecules for uPAR and uPA inhibited invasion by almost 90% at 25 MOI.

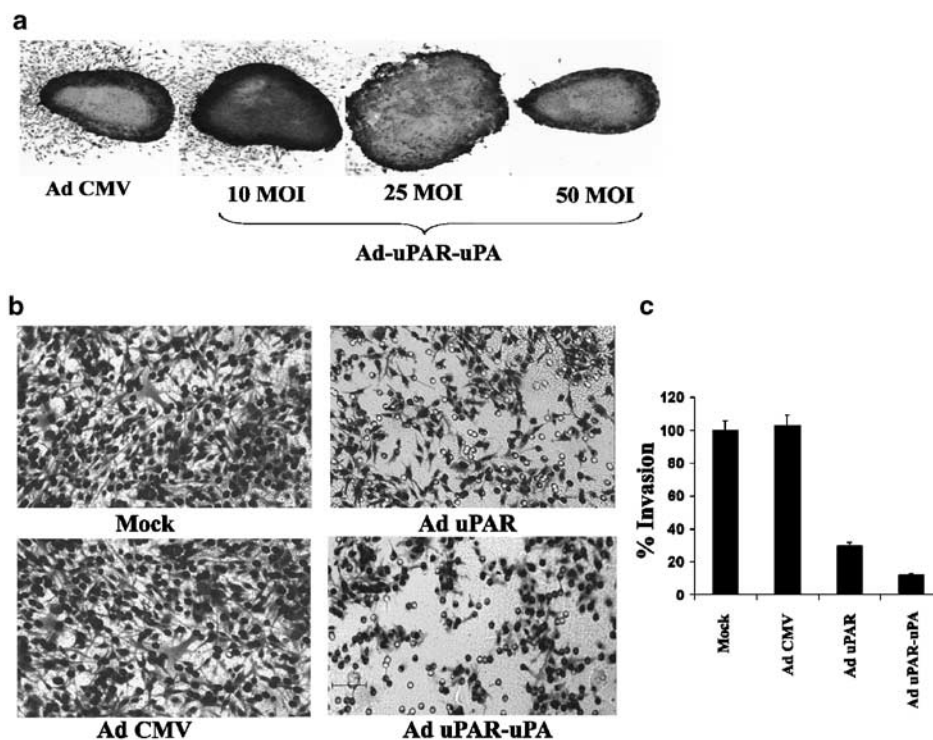


Figure 3 Migration of SNB19 cells infected with Ad-uPAR-uPA or Ad-CMV (a). SNB19 cells (3×10^6 cells) were suspended in DMEM and seeded onto 0.5% agar-coated plates and cultured until spheroids were formed. Spheroids of 100–200 μm in diameter were selected and infected with 5×10^8 PFU of either Ad-CMV or Ad-uPAR-uPA. After 3 days, single glioma spheroids were placed in the center of a vitronectin-coated well in 96-well plate and cultured at 37°C for 48 h. At the end of the migration assay, spheroids were fixed and stained with Hema-3 and photographed (a). Ad-uPAR-uPA infection inhibits invasion of SNB19 cells (b). SNB19 cells were infected with 100 MOI of either Ad-CMV or Ad-uPAR-uPA. After 4 days, 1×10^6 cells were allowed to invade for 24 h through transwell inserts (8 μm pores) coated with Matrigel. The cells that invaded through the Matrigel-coated inserts were stained, counted and photographed under a light microscope at $\times 20$ magnification (b) and invasion was quantified (c) as described in Materials and methods. Data shown are the average values from four separate experiments from each group (\pm s.d.; $P < 0.001$)

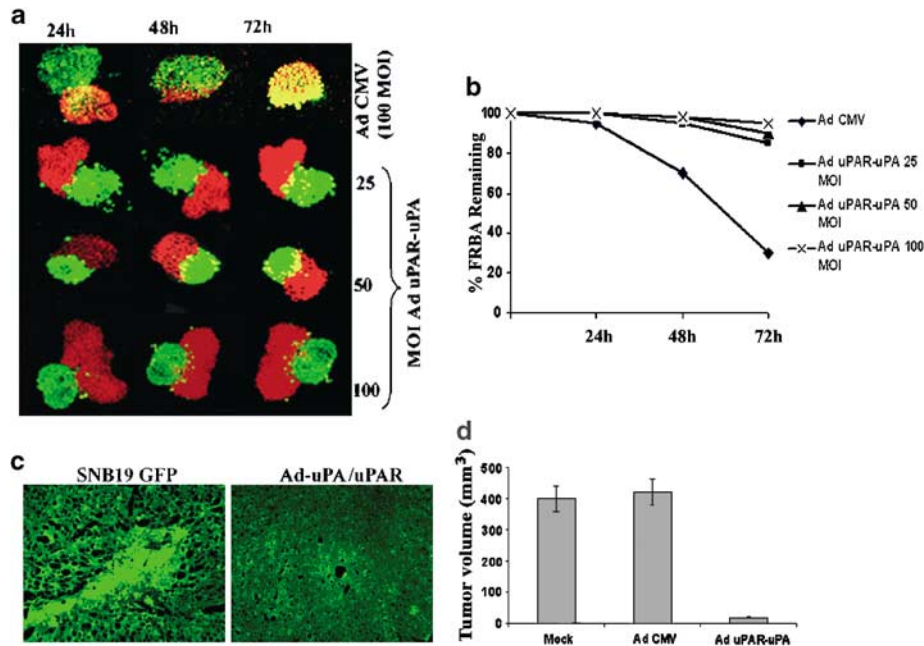


Figure 4 SNB19 cells (3×10^6 cells) were suspended in DMEM and seeded onto 0.5% agar-coated plates and cultured until spheroids formed. Tumor spheroids (red fluorescence) 100–200 μm in diameter were selected, infected with 5×10^8 PFU of Ad-CMV or Ad-uPAR-uPA, and cocultured with fetal rat brain aggregates. After 3 days, progressive destruction of fetal rat brain aggregates (green fluorescence) and invasion of SNB19 cells was observed using confocal laser scanning microscopy (a). Quantification of remaining fetal rat brain aggregates by SNB19 spheroids infected with Ad-CMV or Ad-uPAR-uPA vectors as described in Materials and methods (b). Data shown are the mean \pm s.d. values from four separate experiments for each group ($*P < 0.001$). Tumor growth inhibition of SNB19 GFP cells infected with Ad-uPAR-uPA (c). Ad-uPAR-uPA-infected SNB19 glioblastoma cells, but not those infected with Ad-uPAR, formed intracerebral tumors in nude mice. Cells were infected with PBS or 100 MOI of Ad-uPAR-uPA or Ad-CMV for 4 days, trypsinized, counted and then inoculated intracerebrally (1×10^6 cells in $10 \mu\text{l}$ of PBS) into nude mice (10 mice in each group). The animals were examined for tumor formation over a 5–6-week period and tumor sizes were estimated from tumor sections of GFP expressing cells. Semiquantitation of tumor volume in mock/Ad-CMV- and Ad-uPAR-uPA-infected SNB19 cells 4 weeks after intracranial injection of these cells as described in Materials and methods (d). Data shown are the mean \pm s.d. values from 10 animals from each group ($*P < 0.001$)

Ad-uPAR-uPA inhibited tumor formation and caused tumor regression in nude mice

Having demonstrated that Ad-uPAR-uPA infection decreased migration, invasion, and angiogenesis in SNB19 cells *in vitro*, we investigated the effect of this Ad-uPAR-uPA on the growth of two glioblastoma cell lines in nude mice. An SNB19 variant that expresses green fluorescent protein (GFP) was infected with mock, Ad-CMV or Ad-uPAR-uPA (100 MOI) and then injected intracerebrally into nude mice. All 10 of the mice in each group injected with noninfected cells and Ad-CMV-infected cells developed tumors while none of the animals injected with Ad-uPAR-uPA-infected cells developed tumors over a 4–5 weeks follow-up period (Figure 4c). Quantitation of tumor size showed a significant reduction ($P < 0.001$) in Ad-uPAR-uPA-infected cells compared to mock- and Ad-CMV-infected cells (Figure 4d). This represented more than 40-fold reduction in the tumor volume when compared to untreated controls or Ad-CMV-infected cells. In a separate experiment, 4×10^6 U87 MG glioblastoma cells were injected subcutaneously in nude mice. After the tumors reached 5 mm in diameter (6–8 days), they were injected every third day with a total of three doses of either Ad-CMV or Ad-uPAR-uPA (1×10^9 PFU). All 10

mice with the Ad-uPAR-uPA-injected vector showed tumor regression beginning on the fourth day after the second injection and continuing for 16 days, at which approximately 80% of inhibition was seen relative to the Ad-CMV-injected tumors (Figure 5). By 24 days, inhibition was approximately 95% relative to the subcutaneous tumors that had been injected with the Ad-CMV.

Discussion

In this study we used an Ad-uPAR construct and a bicistronic Ad-uPAR-uPA construct that express either antisense uPAR or antisense uPAR plus antisense uPA to infect SNB19 glioma cells, cultured in the presence or absence of vitronectin, in an attempt to retard the invasiveness of glioma cells. Western blot analysis and zymography confirmed that Ad-uPAR-uPA could significantly downregulate the expression of both uPAR and uPA. The production of pro-uPA and its subsequent activation to uPA by its interaction with uPAR is an important step in glioma cell invasion, as it is required for efficient activation of plasmin to plasminogen and ECM degradation (Ellis and Dano, 1993). The

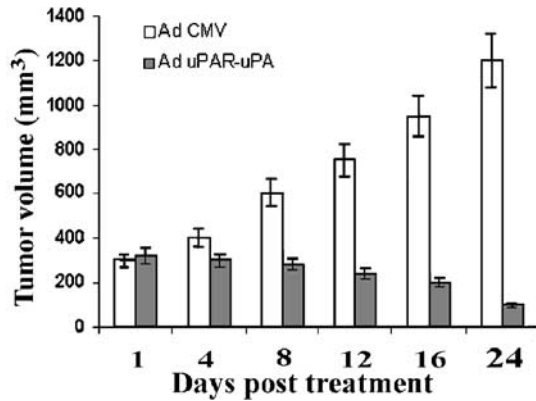


Figure 5 Growth inhibition of pre-established tumors via intratumoral injection of Ad-uPAR-uPA-infected U87 cells (5×10^6) in $100 \mu\text{l}$ of PBS in nude mice. After 8–10 days, the resultant 4–5 mm subcutaneous tumors were injected intratumorally with Ad-CMV (vector control) or Ad-uPAR-uPA (5×10^8 PFU) in a $100\text{-}\mu\text{l}$ volume. A total of four injections were given, one every other day, and the tumor size was measured with calipers. Tumor volumes are shown as mean \pm s.d. ($*P < 0.001$)

downregulation of both uPA and uPAR would be an efficient way to circumvent the possibility of uPAR-independent, uPA-mediated plasminogen activation (Bugge *et al.*, 1996; Carmeliet *et al.*, 1998).

Our immunohistochemical results clearly showed that infecting SNB19 cells with Ad-uPAR or Ad-uPAR-uPA led to a significant reduction in cellular uPAR and uPA levels. The growth characteristics of the cells also seem to have changed; the cell density of the Ad-uPAR-uPA-infected cells was less than that of the control cells (data not shown). This effect could be explained by findings that downregulation of Ad-uPAR causes partial cell arrest in G0/G1 (Fibbi *et al.*, 1998; Aguirre Ghiso *et al.*, 1999; Adachi *et al.*, 2002; Kjoller, 2002). Results of our migration studies showed little or no migration of cells from the spheroids consisting of cells infected with 100 MOI of Ad-uPAR-uPA. However, some migration of cells was seen from the spheroids of cells infected with 100 MOI of Ad-uPAR, suggesting that uPAR and uPA are both required for migration. Moreover, spheroids of cells infected with Ad-uPAR-uPA did not attach to vitronectin-coated surfaces. uPAR is a glycosyl phosphatidylinositol-linked protein that engages in multiple lateral protein–protein interactions (Waltz *et al.*, 1997). In addition to its role in adhesion, uPAR is also associated with many other proteins involved in signal transduction pathways (Kook *et al.*, 1994; Koshelnick *et al.*, 1997; Dumler *et al.*, 1998; Blasi, 1999). A physical association between uPAR and the αv chain of the vitronectin receptor leads to functional interaction of these receptors, suggesting that uPAR directs cytoskeletal rearrangement and cell migration by altering $\alpha v \beta 5$ signaling specificity (Kjoller, 2002). Our findings confirm previous reports that both uPAR and uPA are required for cell migration in a vitronectin environment (Busso *et al.*, 1994). The report of functional coupling between $\alpha v \beta 5$ and ligand-activated uPAR is instrumental in gaining insight into the role of integrins in

uPAR-dependent signaling (Busso *et al.*, 1994). uPAR also has the ability to activate protein kinase C and the formation of diacylglycerol (Busso *et al.*, 1994; Fibbi *et al.*, 1998). As a three-domain protein, uPAR can undergo limited cleavage that exposes a sequence between domains 1 and 2 that has been shown to induce signaling and chemotaxis (Kjoller, 2002). This plasticity of uPAR and its dynamic interaction with adapter proteins may be responsible for the observed multiplicity of signaling pathways and biological outcomes mediated by uPAR (Sturge *et al.*, 2002). The role of uPA in adhesion has been demonstrated by a dose-dependent stimulation of adhesion to vitronectin by single-chain uPA. In addition, adhesion of cells to vitronectin was completely inhibited by EDTA and RGD but was restored to 40% of the control levels in the presence of uPA (Chang *et al.*, 1998). This observation substantiates our findings that spheroids of Ad-uPAR-uPA-infected cells did not attach to vitronectin-coated plates, even after 72 h. Traditionally, integrins have been thought of as the major cellular receptors mediating adhesion (Lafrenie *et al.*, 1992) while vitronectin has been shown to mediate cell migration *in vitro*, suggesting that cells may use vitronectin to adhere and migrate.

The ability of spheroids of Ad-uPAR infected cells to attach and migrate on vitronectin-coated plates and the inability of Ad-uPAR-uPA-infected spheroids to do so may reflect the fact that uPAR and uPA form a feedback loop in which one causes the upregulation of the other. Hence, simultaneous downregulation of both uPA and uPAR would completely block this feedback loop, whereas downregulation of uPAR alone may not, perhaps because of residual amounts of uPAR on the cell surface. uPA is induced not only by uPAR but also by other factors such as insulin growth factor 1, and its induction depends on phosphatidylinositol 3 kinase and MAPK (Siewerts *et al.*, 2002). Thus, the downregulation of both uPAR and uPA may not provide sufficient signaling for other molecules involved in attachment. We also observed that downregulation of both uPAR and uPA retarded the invasiveness of glioma cells through Matrigel, in contrast to the complete lack of migration and attachment of the Ad-uPAR-uPA infected cell spheroids. This difference probably reflects the use of vitronectin for the spheroid migration assay and the use of Matrigel in the invasion assay. Matrigel is a solubilized basement membrane prepared from EHS mouse sarcoma, the major components of which are laminin, collagen IV, heparansulfate-proteoglycans, enactin, and nidogen. Various other components like TGF- β , fibroblast growth factor, tissue plasminogen activator, and other growth factors associated with mouse sarcoma tumors are also present (Kleinman *et al.*, 1982). These other components probably provide the means for attachment to receptors on the cell surface, and thus the means for invasion to occur. The presence of tissue plasminogen activator in Matrigel probably induces the activation of plasmin to plasminogen in order to degrade the Matrigel matrix and facilitate invasion. Our finding that downregulation of both uPA and uPAR reduced the invasiveness of glioma cells

confirms the significance of both uPA and uPAR in the invasive behavior of glioma cells. In the absence of uPA and uPAR, other factors may play a role in invasion and migration, but to a lesser extent.

In this investigation, we successfully targeted both uPAR and uPA, reducing the effect of uPAR-independent activation of uPA and retarding the attachment of glioma cells to the ECM, thereby disabling glioma invasion. The disruption of the interaction between uPAR and uPA at the cell surface is known to block the activation of plasminogen and urokinase, preventing subsequent activation of the proteolytic cascade required for invasion (Estreicher *et al.*, 1990). Previous studies using mice lacking the gene for uPA showed that tumor development is retarded in a uPA-deficient environment (Gutierrez *et al.*, 2000).

Our *in vitro* findings indicated that the simultaneous downregulation of both uPA and uPAR inhibited glioma cell invasiveness and angiogenesis. It has been reported that loss of PAI-1 in the host results in the enhanced adhesion of uPAR-bearing endothelial cells to the ECM protein vitronectin, which adversely affects cell motility and resultant neovascularization (Gutierrez *et al.*, 2000). Moreover, maintaining a balance between cell adhesion and proteolytic-mediated detachment through regulation of uPA activity may be necessary for protecting the neovascular tissue (Gutierrez *et al.*, 2000). Several antagonistic peptides identified by bacteriophage display as blocking uPA binding have been shown to inhibit angiogenesis and primary tumor growth in syngeneic nude mice (Min *et al.*, 1996). In another study, the Ad-mediated expression of a secreted antagonist of murine uPA/uPAR was shown to suppress angiogenesis-dependent tumor growth and dissemination in mice (Li *et al.*, 1998). Our results showed that both uPA and uPAR are required for vascularization. Therefore, a reduction in the levels of these proteins suppresses angiogenesis.

Our *in vivo* findings established that infecting SNB19 cells with Ad-uPAR-uPA prevents those cells from forming tumors after intracranial injection in nude mice and suppresses subcutaneous tumor growth in already established subcutaneous tumors. Conversely, reducing uPAR levels by using antisense oligonucleotides was also found to inhibit tumor growth, invasion and metastasis in some cancers (Kook *et al.*, 1994). Down-regulation of uPAR expression with an antisense strategy produced a protracted period of dormancy in human epidermoid carcinoma cells (Yu *et al.*, 1997). Our previous results indicated that infection of SNB19 cells with Ad-uPAR alone causes the cells to arrest in G0/G1, thereby retarding or suppressing tumor establishment or progression. Although episomal expression of genes through the use of Ad vectors typically does not last for more than a week, intracranial tumors failed to appear even after 5 weeks in our experiments. This finding may reflect a need for the cells to attach to the ECM and become established quickly after injection.

In conclusion, we report that the downregulation of uPAR and uPA effectively reduced the invasiveness, migration, ECM attachment, and angiogenesis of

glioma cells *in vitro* and abrogated the tumorigenicity of these cells *in vivo*. Hence, targeting two components of a single system can have a synergistic effect rather than merely being additive. Taken together, our present data strongly support the therapeutic value of down-regulating uPAR and uPA using an adenovirus bicistronic construct.

Materials and methods

Construction of Ad-uPAR-uPA

We previously constructed an adenovirus expressing an antisense message for the uPAR gene using a pAd-uPAR vector containing a 300-bp DNA fragment of the 5' end of the uPAR gene in the antisense orientation with a CMV promoter and the polyadenylation signal of bovine growth hormone (BGH) (Mohan *et al.*, 1999). This vector was used to construct the Ad-uPAR-uPA bicistronic vector as follows. We subcloned an antisense uPA sequence that was complementary to 1020 bp of the 3' end of the uPA cDNA sequence between the *NotI* and *XhoI* sites of PcDNA3. This fragment was polymerase chain reaction (PCR)-amplified using plaque-forming units (PFU) polymerase-specific primers with *SalI* sites incorporated into the primers (Table 1). The amplified product was digested with *SalI* to generate sticky ends and cloned downstream of the CMV-uPAR-SV40 construct in the Ad-uPAR vector (SV40, simian virus type 40). The sequence of the resulting clone pAd-uPAR-uPA was confirmed and this plasmid construct was cotransfected with the 40–50-kb pJM17 vector into human embryonic kidney 293 cells to isolate recombinant adenoviruses (Graham and Prevec, 1991). Recombinant virus plaques were identified and amplified by PCR using primers specific for CMV and SV40 polyadenylation signals. The recombinant virus was purified by ultracentrifugation in cesium chloride step gradients (Graham and Prevec, 1991). The direction of orientation was determined by partial sequencing from the end of the uPAR antisense sequence. Clones with antisense uPAR and antisense uPA in the same direction were used. The viral DNA was also sequenced to confirm the configuration of the expression cassette. The control virus Ad-CMV has a CMV promoter and a BGH polyadenylation signal but no gene insert in the E1-deleted region.

Cell culture and infection conditions

We used the established human glioma cell line SNB19 for this study. Cells were grown in Dulbecco's modified Eagle medium/F12 medium (1:1, v/v) supplemented with 10% fetal calf serum in a humidified atmosphere containing 5% CO₂ at 37°C. Viral stocks were suitably diluted in serum-free medium to obtain the desired MOI or PFU and added to cell monolayers and tumor cell spheroids (1ml/60mm dish or 3ml/100mm dish) and incubated at 37°C for 30 min. The

Table 1 Primers used for the amplification of *SalI*-CMV-uPA-SV40-*SalI* antisense expression cassette

Forward primer
5' CTGGT <u>GTCGAC</u> CTGCTTCCGCGATGTACGGGC 3'
Reverse primer
5' CTGGT <u>GTCGAC</u> ATCCCCAGCATGCCTGCTAT 3'

necessary amount of culture medium with 10% fetal calf serum was added and the cells were incubated for the desired periods.

Immunoblot analysis

Total cell lysates were prepared in extraction buffer containing Tris (0.1 M (pH 7.5)), Triton-X114 (1.0%), EDTA (10 mM), aprotinin, and phenylmethylsulfonyl fluoride as described previously (Mohan *et al.*, 1999). The extracts were incubated at 37°C for 5 min and centrifuged to separate the lower (detergent) phase that contains mainly hydrophobic membrane proteins including the glycosylphosphatidylinositol-anchored uPAR. Subsequently 20 µg of protein from these samples was separated under nonreducing conditions by 15% SDS-PAGE and transferred to nitrocellulose membranes (Schleicher & Schuell, Keene, NH, USA). The membranes were probed with polyclonal antibodies to uPAR (399 American Diagnostics, Inc., Greenwich, CT, USA) and secondary antibodies (anti-rabbit-horseradish peroxidase) as required and developed according to the enhanced chemiluminescence protocol (Amersham, Greenwich, CT, USA). For loading control, samples were SDS-PAGE-separated under reducing conditions and probed with monoclonal antibodies for β-actin.

Zymography

SNB19 cells were infected with the indicated MOI of Ad-CMV, Ad-uPAR, or Ad-uPAR-uPA. The conditioned media and the cell extracts were collected, and fibrin zymography was used to detect uPA as previously described (Yamamoto *et al.*, 1994). Fibrin zymograms were prepared with the conditioned media as described previously (Chintala *et al.*, 1998).

Immunohistochemical analysis

SNB19 cells (1×10^4 /well) were seeded on vitronectin-coated eight-well chamber slides, incubated for 24 h, and infected with 100 MOI of Ad-CMV, Ad-uPAR, or Ad-uPAR-uPA. After another 72 h, cells were fixed with 3.7% formaldehyde and incubated with 1% bovine serum albumin in phosphate-buffered saline (PBS) at room temperature for 1 h for blocking. After the slides were washed with PBS, either mouse IgG anti-uPAR (rabbit) or IgG anti-uPA (mouse) was added at a concentration of 1:500, and the slides were incubated at room temperature for 1 h and washed three times with PBS to remove excess primary antibody. Cells were then incubated with anti-mouse Texas red conjugate or anti-rabbit fluorescein-5-isothiocyanate (FITC) conjugate IgG (1:500 dilution) for 1 h at room temperature and then washed three times. The slides were covered with glass coverslips and fluorescent photomicrographs were taken.

In vitro angiogenesis assay

SNB19 cells (2×10^4 /well) were seeded in eight-well chamber slides and infected with the indicated MOI of Ad-CMV, Ad-uPAR, or Ad-uPAR-uPA. After 24 h of incubation, the medium was removed, 4×10^4 human dermal endothelial cells were added, and the cells were allowed to coculture for 72 h. Cells were then fixed in 3.7% formaldehyde, blocked with 2% bovine serum albumin, and the endothelial cells were stained with factor VIII antigen (DAKO Corp., Carpinteria, CA, USA). The cells were then washed with PBS and incubated with an FITC-conjugated secondary antibody for 1 h. The cells were washed and the formation of tubular capillary-like structures, an indicator of angiogenesis, was assessed by confocal scanning laser microscopy.

Migration of Cells from Spheroids

Migration was assayed according to a previously described method (Mohan *et al.*, 1999) with modifications. Spheroids of SNB19 cells were prepared by seeding a suspension of 2×10^6 cells in Dulbecco's modified Eagle medium on 100 mm tissue culture plates coated with 0.75% agar and culturing them until spheroid aggregates formed. Spheroids measuring $\sim 150 \mu\text{m}$ in diameter (about 4×10^4 cells/spheroid) were selected and infected with PBS (mock condition) or adenovirus vectors (Ad-CMV, Ad-uPAR, or Ad-uPAR-uPA) at 100 MOI. At 3 days after infection, a single glioma spheroid was placed in the center of each well in vitronectin-coated 96-well microplates, and 200 µl of serum-free medium was added to each well. Spheroids were cultured at 37°C for 72 h, after which the spheroids were fixed and stained with Hema-3, and cellular migration from the spheroids was assessed under light microscopy.

Matrigel invasion assay

Invasion of glioma cells *in vitro* was measured by the invasion of cells through Matrigel-coated (Collaborative Research, Inc., Boston, MA, USA) transwell inserts (Costar, Cambridge, MA, USA). Briefly, transwell inserts with 8 µm pores were coated with a final concentration of 1 mg/ml of Matrigel, cells were trypsinized, and 200 µl aliquots of cell suspension (1×10^6 cells/ml) were added in triplicate wells. After a 24 h incubation, cells that passed through the filter into the lower wells were quantified as described elsewhere (Mohan *et al.*, 1999; Mohanam *et al.*, 1993) and expressed as a percentage of the sum of cells in the upper and lower wells. Cells on the lower side of the membrane were fixed, stained with Hema-3, and photographed.

Glioma Spheroids

Multicellular spheroids consisting of SNB19 cells were cultured in 35 mm Petri dishes base-coated with 0.75% Noble agar prepared in Dulbecco's modified Eagle medium. Briefly, 3×10^6 cells were suspended in 10 ml of medium, seeded onto the plates, and cultured until spheroids formed. Spheroids, 100–200 µm in diameter, were selected and infected with the indicated MOI of Ad-CMV, Ad-uPAR, or Ad-uPAR-uPA. At 3 days after infection, tumor spheroids were stained with the fluorescent dye 1'-dioctadecyl-3,3,3',3'-tetramethylindocarbocyanine perchlorate (DiI) and confronted with fetal rat brain aggregates that were stained with 3,3'-dioctadecyloxycarbocyanine perchlorate (DiO). The progressive destruction of fetal rat brain aggregates and invasion of SNB19 cells were observed by phase contrast microscopy and photographed as described previously (Go *et al.*, 1997).

Animal experiments

For the intracerebral tumor model, SNB19 cells that express GFP were infected in culture with PBS (mock), Ad-CMV, or Ad-uPAR-uPA (100 MOI) for 5 days, trypsinized, counted, and intracerebrally inoculated into nude mice. Six mice were killed 4 weeks after tumor inoculation from each group by cardiac perfusion with paraformaldehyde, their brains were removed, and frozen sections were prepared and observed for GFP fluorescence. The 3–5 µm sections were blindly reviewed and scored semiquantitatively for the size of the tumor in each case. The average cross-sectional diameter was used to calculate tumor size and compared between the controls and treated groups. The variation between the sections in each group was less than 10% for the tumor regression experiments.

U87MG cells (5×10^6 cells) were subcutaneously injected into nude mice. After 8 days, when tumors had reached 4–5 mm in diameter, the mice were injected with PBS (mock), Ad-CMV, or Ad-uPAR-uPA (5×10^8 PFU) intratumorally every other day for a total of five injections. Tumor size was measured every second day and tumor volume was calculated from the formula $1/6\pi (R_{\max})^2 \times (R_{\min})^2$, where R_{\max} and R_{\min} are the maximum and minimum tumor radii, respectively.

Abbreviations

uPA, urokinase-type plasminogen activator; Urokinase-type

plasminogen receptor (uPAR); Ad, adenovirus; CMV, cytomegalovirus; BGH, bovine growth hormone; SV40, simian virus type 40; PCR, polymerase chain reaction; MOI, multiplicities of infection; PFU, plaque-forming units; PBS, phosphate-buffered saline; FITC, fluorescein-5-isothiocyanate; DiI, 1'-dioctadecyl-3,3,3',3'-tetramethylindocarbocyanine perchlorate; DiO, 3,3'-dioctadecyloxycarbocyanine perchlorate; GFP, green fluorescent protein; ECM, extracellular matrix; PAR, plasminogen activator receptor.

Acknowledgements

We thank Karen Minter for preparation of the manuscript.

References

- Adachi Y, Chandrasekar N, Kin Y, Lakka SS, Mohanam S, Yanamandra N, Mohan PM, Fuller GN, Fang B, Fueyo J, Dinh DH, Olivero WC, Tamiya T, Ohmoto T, Kyritsis AP and Rao JS. (2002). *Oncogene*, **21**, 87–95.
- Adachi Y, Lakka SS, Chandrasekar N, Yanamandra N, Gondi CS, Mohanam S, Dinh DH, Olivero WC, Gujrati M, Tamiya T, Ohmoto T, Kouraklis G, Aggarwal B and Rao JS. (2001). *J. Biol. Chem.*, **276**, 47171–47177.
- Aguirre Ghiso JA, Alonso DF, Farias EF, Gomez DE and Kier Joffe EB. (1999). *Eur. J. Biochem.*, **263**, 295–304.
- Blasi F. (1999). *APMIS*, **107**, 96–101.
- Bugge TH, Flick MJ, Danton MJ, Daugherty CC, Romer J, Dano K, Carmeliet P, Collen D and Degen JL. (1996). *Proc. Natl. Acad. Sci. USA*, **93**, 5899–5904.
- Busso N, Masur SK, Lazega D, Waxman S and Ossowski L. (1994). *J. Cell Biol.*, **126**, 259–270.
- Carmeliet P, Moons L, Dewerchin M, Rosenberg S, Herbert JM, Lupu F and Collen D. (1998). *J. Cell Biol.*, **140**, 233–245.
- Chang AW, Kuo A, Barnathan ES and Okada SS. (1998). *Arterioscler. Thromb. Vasc. Biol.*, **18**, 1855–1860.
- Chintala SK, Sawaya R, Aggarwal BB, Majumder S, Giri DK, Kyritsis AP, Gokaslan ZL and Rao JS. (1998). *J. Biol. Chem.*, **273**, 13545–13551.
- Dumler I, Weis A, Mayboroda OA, Maasch C, Jerke U, Haller H and Gulba DC. (1998). *J. Biol. Chem.*, **273**, 315–321.
- Ellis V and Dano K. (1993). *J. Biol. Chem.*, **268**, 4806–4813.
- Estreicher A, Muhlhauser J, Carpentier JL, Orci L and Vassalli JD. (1990). *J. Cell Biol.*, **111**, 783–792.
- Fibbi G, Caldini R, Chevanne M, Pucci M, Schiavone N, Morbidelli L, Parenti A, Granger HJ, Del Rosso M and Ziche M. (1998). *Lab. Invest.*, **78**, 1109–1119.
- Foekens JA, Look MP, Peters HA, van Putten WL, Portengen H and Klijn JG. (1995). *J. Natl. Cancer Inst.*, **87**, 751–756.
- Go Y, Chintala SK, Mohanam S, Gokaslan Z, Venkaiiah B, Bjerkvig R, Oka K, Nicolson GL, Sawaya R and Rao JS. (1997). *Clin. Exp. Metastasis*, **15**, 440–446.
- Graham FL and Prevec L. (1991). *Methods in Molecular Biology*. Murray EJ (ed). The Humana Press: Clifton, NJ, pp. 109–127.
- Gutierrez LS, Schulman A, Brito-Robinson T, Noria F, Ploplis VA and Castellino FJ. (2000). *Cancer Res.*, **60**, 5839–5847.
- Kjoller L. (2002). *Biol. Chem.*, **383**, 5–19.
- Kleinman HK, McGarvey ML, Liotta LA, Robey PG, Tryggvason K and Martin GR. (1982). *Biochemistry*, **21**, 6188–6193.
- Kobayashi H, Moniwa N, Sugimura M, Shinohara H, Ohi H and Terao T. (1993). *Jpn. J. Cancer Res.*, **84**, 633–640.
- Kook YH, Adamski J, Zelent A and Ossowski L. (1994). *EMBO J.*, **13**, 3983–3991.
- Koshelnick Y, Ehart M, Hufnagl P, Heinrich PC and Binder BR. (1997). *J. Biol. Chem.*, **272**, 28563–28567.
- Lafrenie RM, Podor TJ, Buchanan MR and Orr FW. (1992). *Cancer Res.*, **52**, 2202–2208.
- Li H, Lu H, Griscelli F, Opolon P, Sun LQ, Ragot T, Legrand Y, Belin D, Soria J, Soria C, Perricaudet M and Yeh P. (1998). *Gene Therapy*, **5**, 1105–1113.
- Min HY, Doyle LV, Vitt CR, Zandonella CL, Stratton-Thomas JR, Shuman MA and Rosenberg S. (1996). *Cancer Res.*, **56**, 2428–2433.
- Mohan PM, Chintala SK, Mohanam S, Gladson CL, Kim ES, Gokaslan ZL, Lakka SS, Roth JA, Fang B, Sawaya R, Kyritsis AP and Rao JS. (1999). *Cancer Res.*, **59**, 3369–3373.
- Mohanam S, Sawaya R, McCutcheon I, Ali-Osman F, Boyd D and Rao JS. (1993). *Cancer Res.*, **53**, 4143–4147.
- Nielsen LS, Hansen JG, Skriver L, Wilson EL, Kaltoft K, Zeuthen J and Dano K. (1982). *Biochemistry*, **21**, 6410–6415.
- Park IK, Kim BJ, Goh YJ, Lyu MA, Park CG, Hwang ES and Kook YH. (1997). *Int. J. Cancer*, **71**, 867–873.
- Sappino AP, Busso N, Belin D and Vassalli JD. (1987). *Cancer Res.*, **47**, 4043–4046.
- Schmitt M, Janicke F, Moniwa N, Chucholowski N, Pache L and Graeff H. (1992). *Biol. Chem. Hoppe Seyler*, **373**, 611–622.
- Siewewerts AM, Martens JW, Dorssers LC, Klijn JG and Foekens JA. (2002). *Thromb. Haemost.*, **87**, 674–683.
- Sturge J, Hamelin J and Jones GE. (2002). *J. Cell Sci.*, **115**, 699–711.
- Waltz DA, Natkin LR, Fujita RM, Wei Y and Chapman HA. (1997). *J. Clin. Invest.*, **100**, 58–67.
- Yamamoto M, Sawaya R, Mohanam S, Bindal AK, Bruner JM, Oka K, Rao VH, Tomonaga M, Nicolson GL and Rao JS. (1994a). *Cancer Res.*, **54**, 3656–3661.
- Yamamoto M, Sawaya R, Mohanam S, Rao VH, Bruner JM, Nicolson GL and Rao JS. (1994b). *Cancer Res.*, **54**, 5016–5020.
- Yu W, Kim J and Ossowski L. (1997). *J. Cell Biol.*, **137**, 767–777.